ELSEVIER

Contents lists available at ScienceDirect

# Journal of Water Process Engineering

journal homepage: www.elsevier.com/locate/jwpe



# Ultra-high sulfate loads and iron precision dosing for hydrogen sulfide management: A mass balance assessment and microbial structure implications in anaerobic bioreactors

Valentina Girardi <sup>a,b</sup>, María Laura Tondo <sup>a,b</sup>, Cecilia Lucía Balaban <sup>a,b</sup>, María Sol Herrero <sup>a</sup>, Camila Olivera <sup>a,b</sup>, Lucas Matías Salvatierra <sup>a,b,\*</sup>

### ARTICLE INFO

Editor: Li Gao

Keywords: Biogas Sulfate Hydrogen sulfide SRB

#### ABSTRACT

This article presents an original and detailed study of semi continuous lab-scale anaerobic bioreactors subjected to Sulfate Loads Rates (SLRs)  $>130~mgSO_4^2/day.L_{reactor}$ . At these sulfate inputs, hydrogen sulfide yield by bacterial conversion can reach concentrations above 400 mg/L in the liquid phase and more than 25,000 ppm in gas phase, respectively. Both values comprise significant technical challenges in biogas plants as well as health and environmental concerns.

In order to control sulfide in liquid phase, two bioreactors were treated with opposite ferric dosing strategies: one underwent five consecutive cycles of shock precipitation of hydrogen sulfide, reducing peak levels from  $\sim\!400$  mg/L to  $<\!40$  mg/L; the other involved the application of a more continuous and fine-tuned dosing strategy to manage sulfide concentrations across different stepwise levels: 400–300, 300–200, 200–100, and 100 to  $<\!10$  mg/L. A third bioreactor, without iron addition, stabilized at  $\sim\!250$  mg/L H<sub>2</sub>S and 10,000 ppm in biogas over 140 days. A detailed sulfur mass balance enabled analysis of sulfate-to-sulfide conversion rates, Henry's constants between liquid and gas phases, and  ${\rm Fe^{3^+}/S^{2^-}}$  molar ratios for both strategies. Values of 0.99 and 0.65 were obtained, matching with the stoichiometry of FeS during shock precipitation and FeS +  ${\rm S^0}$  and/or Fe<sub>2</sub>S<sub>3</sub> in stepwise precipitation, respectively. High-throughput sequencing of the 16S rRNA gene revealed subtle yet significant changes in the microbial community structures within bioreactors subjected to high sulfate loads and iron addition. Furthermore, the authors characterized the late-stage microbial response following methanogenic process inhibition and the cessation of biogas production.

## 1. Introduction

In the circular-economy context, agro-industrial effluents are valuable resources, with many components upcyclable into other products through green chemistry or fermentation. When these strategies are unfeasible, anaerobic digestion (AD) remains an effective alternative, recovering chemical energy from organic matter and reducing the environmental impact of effluent discharge. However, certain agro-industrial wastewaters with high sulfate concentrations pose challenges for AD bioreactor stability. Sulfate stimulates the dissimilative sulfur pathway, promoting sulfate-reducing bacteria (SRB) that compete with methanogens for key substrates. SRB use hydrogen and low

molecular weight organic compounds as electron donors to reduce sulfate to sulfide (Eq. (1)), which inhibits methane production and reduces the efficiency of biogas generation [1].

Hydrogen sulfide in aqueous solutions exists in three forms: non-ionized  $H_2S_{liq}$ , ionized bisulfide  $H_S_{liq}$ , and  $S_{liq}^2$ , depending on pH and temperature [2]. Non-ionized  $H_2S_{liq}$ , predominant at pH <7 (pKa<sub>1</sub> = 6.99 at 25 °C), is particularly toxic to methanogenic archaea and other microorganisms due to its ability to diffuse across microbial cell membranes and inhibit metabolic activity [1]. This often results in the accumulation of intermediates, such as volatile fatty acids (VFAs), acidifying the bioreactor and reducing Chemical Oxygen Demand (COD) removal efficiency, leading to system failure [3]. In contrast,  $S_{liq}^{2}$ 

<sup>&</sup>lt;sup>a</sup> Instituto de Investigaciones en Ingeniería Ambiental, Química y Biotecnología Aplicada – INGEBIO-, Facultad de Química e Ingeniería del Rosario, Pontificia Universidad Católica Argentina (UCA), Av. Pellegrini 3314 (S2002QEO), Rosario, Santa Fe, Argentina

Consejo Nacional de Investigaciones Científicas y Técnicas (CONICET), Argentina

<sup>\*</sup> Corresponding author at: Av. Pellegrini 3314 (S2002QEO), Rosario, Santa Fe, Argentina. E-mail address: lucas salvatierra@uca.edu.ar (L.M. Salvatierra).

concentration in aqueous solutions is negligible under typical conditions (pKa $_2=14.6$  at 25  $^{\circ}$ C) [4].

To counteract sulfide formation and its side effects, several strategies are employed, including micro-aeration [5], and the addition of iron compounds to precipitate insoluble sulfides [6]. Iron salts are particularly effective, as their cations not only remove sulfides from both the liquid phase and biogas [7] but also enhance methanogenesis by providing essential trace elements for methanogenic archaea growth [8]. In this scenario, ferrous cations (Fe<sup>2+</sup>) react directly with bisulfide (HS $\bar{l}iq$ ) to form ferrous sulfide (FeS), as shown in Eq. (2). Conversely, ferric cations (Fe<sup>3+</sup>) must first be reduced to their ferrous form before precipitating as sulfide. This reduction can occur chemically, through the oxidation of bisulfide to elemental sulfur (S<sup>0</sup>), as described in Eq. (3) [9], or biologically, via chemoautotrophic bacteria that use Fe<sup>3+</sup> as a terminal electron acceptor. Alternatively, Fe<sup>3+</sup> can also react with bisulfide to form ferric sulfide, as indicated in Eq. (4) [6].

$$SO_4^{-2} + 2H^+ \leftrightarrow H_2S + 2O_2$$
 (1)

$$Fe^{2+} + HS^- \leftrightarrow FeS + H^+$$
 (2)

$$2Fe^{3+} + HS^{-} \leftrightarrow 2Fe^{2+} + S^{0} + H^{+}$$
 (3)

$$2Fe^{3+} + 3HS^- \leftrightarrow 2Fe_2S_3 + 3H^+$$
 (4)

To effectively implement this strategy, iron dosing must align with the sulfide levels present in the bioreactor's liquid phase. However, determining the optimal dosage is influenced by several interacting factors—such as pH, redox potential, and temperature—that interact in complex, partially understood ways, often causing deviations from the stoichiometric relationships in Eqs. (2), (3), and (4) [6,10]. Among ferric salts, FeCl<sub>3</sub> is particularly advantageous due to its high solubility in aqueous solutions (0.92 g/mL at 20 °C), cost-effectiveness, and its ability to retard dissimilatory sulfate reduction by acting as an alternative electron acceptor [11]. In aqueous environments, FeCl<sub>3</sub> forms an acidic Fe(OH)<sub>3</sub> dispersion that readily reacts with sulfides to precipitate insoluble iron sulfides. Recommended dosages, according to Erdirencelebi and Kucukhemek [12], range between 1.17 and 3.5 g of Fe<sup>3+</sup> per gram of sulfide precipitated.

Despite extensive research, to the best of the authors' knowledge, no comprehensive study has yet been conducted on sulfur tracking and sulfide control in biogas reactors subjected to SLRs exceeding 100  $\rm mgSO_4^{2-}/day.L_{reactor}.$  Under anaerobic conditions, such sulfate overloads can yield sulfides above 400 mg/L in the liquid phase and  $\rm H_2S$  levels exceeding 25,000 ppm in biogas. These values involve critical technical challenges in biogas plants as well as health and environmental concerns.

In a previous study, the authors explored the early-stage response of lab-scale biogas reactors to multiple SLRs using a sulfate-rich agro-industrial effluent [13]. A detailed discussion on  $\rm H_2S$  in biogas was presented, addressing sulfur input, the quantification of volatile sulfide compounds (VSCs) and the resulting changes in the microbial community.

In the present article, the authors investigated the long-term effects of bioreactor instability caused by inhibition and acidification when exposed to SLR up to 136.1 mgSO $_4^2$ /day.L $_{\rm reactor}$ . More important, two sulfide precipitation strategies were assessed in separate bioreactors: one involving periodic shock precipitation, and the other applying a continuous, stepwise dosing approach. A third bioreactor, used as a control, was stabilized at a lower SLR (71.83 mgSO $_4^2$ /day.L $_{\rm reactor}$ )—nearly half that of the treated systems—for over 140 days without Fe $^{3+}$  addition. The study evaluated sulfate-to-sulfide conversion, Henry's constants for liquid-gas phase transfer, and Fe $^{3+}$ /S $^{2-}$  molar and mass ratios across different conditions and dosing strategies. Microbiological structure of the ferric-treated bioreactors and the late-stage response after methanogenic inhibition and biogas cessation were also examined. High throughput 16S rRNA sequencing and bioinformatics analysis

revealed subtle yet compelling shifts in microbial community composition among diverse conditions.

### 2. Materials and methods

### 2.1. Analytical techniques

All samples were transported to the laboratory under refrigeration and protected from light and air exposure. COD, pH, sulfide and sulfate determinations were carried out according to APHA Standard Methods [14]. For sulfide quantification, the procedure specifically targeted the dissolved fraction, including the non-ionized and ionized forms ( ${\rm H}_2{\rm S}_{liq}/{\rm HS}_{liq}$ ) but not insoluble sulfides. To this end, samples were centrifuged at 7000g for 5 min, and the resulting supernatant was utilized for analysis.

### 2.2. Collection of inoculum and substrates

The inoculum was sourced from a local biogas facility processing agro-industrial liquid residues from vegetable oils, biodiesel, dairy, and food industries. It was seeded into lab-scale bioreactors and stabilized for over two weeks prior to the experiments, preserving the original multi-feed composition and the Organic Load Rate (OLR) of 2000 mgCOD/day. $L_{\rm reactor}$ .

The Sulfate Substrate (SS) was wastewater obtained from a local company producing vegetable olein (i.e., a mixture of fatty acids derived from the chemical refining of soybean and sunflower oils), making it suitable for biogas-based energy recovery due to its high organic COD (Table 1). However, it also contains sulfate concentrations typically between 15,000–25,000 mgSO $_{\rm s}^{2}$ /L, being strongly acidic (pH  $\sim$ 2). Main organic components include mono-, di-, and triglycerides, free glycerol, fatty acids, and phospholipids.

Conversely, the Base Substrate (BS), serving as both background and diluent, consisted of the same wastewater mixture fed to the biogas plant from which the microbial inoculum was sourced. Mainly derived from vegetable oil processing and the biodiesel industry, the BS contains low sulfate concentrations ( $<300~\text{mgSO}_4^2$ /L) (Table 1).

# 2.3. Experimental setup

Experiments were carried out in three 10 L lab-scale bioreactors made of borosilicate glass and PTFE (Figmay, Córdoba, Argentina). Each unit included a brushless motor driving a vertical paddle stirrer (0–120 rpm), and a jacketed electric heating system with a PT100 probe and PID controller (Novus LogBox, Brazil) to set temperatures up to 80 °C. Digesters featured a bottom valve for solids discharge, a Graham condenser for biogas collection in  $10\,\mathrm{L}$  Tedlar® bags, and a top port with a rubber stopper allowing feeding and digestate removal via peristaltic pumps. Reactors ran in semi-continuous mode under constant agitation and temperature control.

### 2.4. Bioreactor operation

Each bioreactor was loaded with 8.5 L of inoculum, leaving a 1.5 L headspace. Systems operated at 55 rpm and 31  $\pm$  1  $^{\circ}\text{C}$  (mesophilic conditions). Daily, digestate was extracted to maintain a constant liquid volume, followed by the corresponding feed addition. Biogas production was registered each day using the liquid displacement method by the gas

Physicochemical parameters of the inoculum (I) and substrates: base substrate (BS) and sulfate-rich substrate (SS).

	COD (mg/L)	pН	Total S (mg/L)	Sulfide (mg/L)	Sulfate (mg/L)
I	1300	7.5	16.3	~4	49
BS	67,027	5.0	84.7	<1	254
SS	237,623	1.7	6214	<1	18,620

collected in Tedlar® bags, while its composition (% $CH_4$ , % $CO_2$ , % $O_2$  and  $H_2S$  concentration) was determined using an Optima 7 Biogas Analyzer (MRU Instruments, USA). To operate within the instrument's  $H_2S$  detection limit of 2000 ppm, dilutions with  $N_2$  5.0 (Linde, Argentina) were conducted when necessary, using high-volume gas-tight syringes (Hamilton, USA). All syringes, connectors, and tubing were made of glass and PTFE to maintain integrity and prevent contamination.

During the startup and stabilization phase, all bioreactors, named R1, R2, and R3, were uniformly fed with BS. The OLR was gradually increased from 0 to 2000 mgCOD/day. $L_{reactor}$  over the first two weeks. After 15 additional days of stabilization, "day zero" was established, marking the beginning of new feeding compositions for R1 and R2, as shown in Table 2. From that point, while maintaining a constant OLR, R1 was fed entirely with SS, whereas R2 received an equal COD contribution from SS and BS—corresponding to approximately 50 % of R1's SLR. On day #43, R3 also transitioned from BS to 100 % SS.

R2 served as an untreated reference, operating without iron addition. R1 was subjected to a shock ferric dosing strategy, aimed to promptly reduce peak sulfide concentrations from ~400 mg/L to <40 mg/L. In contrast, from day #82 onward, R3 followed a stepwise ferric dosing approach, to manage sulfide levels between: 400 to 300, 300 to 200, 200

mass 
$$S_{out \ liq} = Vol_{out \ liq} \left\{ \left[ SO_4^{2-} \right]_{out \ liq} * \frac{MW \ S}{MW \ SO_4^{2-}} + \left[ H_2 S/H S^- \right]_{out \ liq} * \frac{MW \ S}{MW \ H_2 S/H S^-} \right\}$$

$$(6)$$

The **sulfur released in the biogas** was calculated by using the daily biogas volume and the measured  $H_2S_g$  volumetric concentration, assuming ideal gas behavior (Eq. (7)). As before, it can be integrated over a time interval and then averaged per day.

$$mass S_{out g} = MW S^* n_{H_s S_g} = MW S^* \frac{P^* V_{H_s S_g}}{RT} = MW S^* \frac{P^* V_{biogas}^* [H_s S]_g}{RT}$$
(7)

where  $P = 1.013 * 10^5 \, \text{Pa}$  (1 atm),  $T = 298 \, \text{K}$ ,  $MWS = 32.06 \, \text{g} * \text{mol}^{-1}$ ,  $R = 8.314 \, \text{J} * \text{K}^{-1} * \text{mol}^{-1}$  and n is the number of moles (i.e., 1 mol of S per mol of  $H_2S_0$ ).

The **changes in sulfur content within the bioreactor** were calculated by comparing two different days (e.g.,  $t_2$  and  $t_1$ ), based on the S mass variations related to the  $SO_4^{2-}$  and  $H_2S_{liq}/HS_{liq}^{-}$  concentrations over the entire liquid bioreactor's volume (Eq. (8)).

$$\Delta mass \, S_{R_{t_1}^{t_2}} = Vol_R * \Delta \left\{ \left[ \, SO_4^{2-} \right]_{out \, liq} * \frac{MW \, S}{MW \, SO_4^{2-}} + \left[ \, H_2 S/HS^- \right]_{out \, liq} * \frac{MW \, S}{MW \, H_2 S/HS^-} \right\}_{t_1}^{t_2}$$
(8)

to 100, and 100 to <10 mg/L). Both protocols employed a 10 % w/v FeCl<sub>3</sub>·6H<sub>2</sub>O stock solution.

### 2.5. Sulfur mass balance. Calculations

The analysis monitored the sulfur input, as sulfate  $(SO_4^{2-})$ , its conversion to sulfides, and—when iron was added—the estimative formation of iron sulfides  $(Fe_xS_y)$ . Changes within the bioreactors and outputs from the system—either as  $SO_4^{2-}$  or  $H_2S_{liq}/HS_{liq}^{-}$  in the digestate, or as  $H_2S_g$  in the biogas—were quantified.

To determine the **sulfur mass input**, the concentration of  $SO_4^{2-}$  in each feed substrate was measured. The result was then multiplied by the daily feed volume and expressed in terms of atomic sulfur mass (Eq. (5)). SLR can then be obtained by dividing this value by the bioreactor volume.

mass 
$$S_{in\ liq} = Vol_{in\ liq} * [SO_4^{2-}]_{in\ liq} * \frac{MWS}{MWSO_2^{2-}}$$
 (5)

The total **sulfur mass output in the liquid phase** (i.e., digestate) was estimated by quantifying both  $SO_4^{2-}$  and  $H_2S_{liq}/HS_{liq}^-$  concentrations in the daily purged volumes, expressed in terms of atomic S, and added as shown in Eq. (6). As measurements were not performed daily, interpolation was applied when necessary to estimate the intermediate values.

**Table 2**Feeding composition and applied loads from day zero in each reactor.

Feeding parameter	R1	R2	R3 ( <day #43)</day 	R3 (≥day #43)
OLR (mgCOD/day.L <sub>reactor</sub> )	2000	2000	2000	2000
% vol SS/BS	100/ 0	20/ 80	0/100	100/0
% COD contribution (SS/ BS)	100/ 0	50/ 50	0/100	100/0
SLR (mgSO <sub>4</sub> <sup>2-</sup> /day.L <sub>reactor</sub> )	136.1	71.83	7.58	136.1

As in Eq. (5), the values obtained from Eqs. (6) and (7) can be accumulated over a time interval, as outlined in Eq. (8). These accumulated values can then be expressed on a per-day basis and further normalized by the bioreactor volume to enable future work comparisons.

Therefore, the **mass balance analysis** involved the integration between two different days (whether consecutive or not) by comparing the results of the sum of quantities from Eq. (5) with the sum of Eqs. (6), (7) and (8) over the same period.

$$\sum_{t1}^{t2} mass \, S_{in \, liq} = \sum_{t1}^{t2} mass \, S_{out \, liq} + \sum_{t1}^{t2} mass \, S_{out \, g} + \Delta mass \, S_{R_{t_1}^{t_2}}$$
 (9)

In iron-treated bioreactors, an imbalance arose in Eq. (9). The unrecovered sulfur mass on the right side of Eq. (9) was assumed to be precipitated and was then compared to the amount of  ${\rm Fe}^{3+}$  added. Nonetheless, a more accurate and direct relationship was obtained by comparing sulfide concentrations on the same day—immediately before and 1 h after  ${\rm Fe}^{3+}$  addition—based on two independent measurements.

### 2.6. Henry's constant calculations

Henry's constant was calculated based on the concentration of nonionized hydrogen sulfide in the liquid phase. As previously mentioned, the methylene blue method yields total dissolved sulfide concentration (i.e., the sum of both non-ionized  $H_2S_{liq}$  and ionized or bisulfide form  $HS_{liq}$ ). This equilibrium is primarily influenced by pH and temperature, while conductivity plays a minor role [2]. Therefore, at a given temperature, the molar ratio between both species is given by Eq. (10).

$$log \frac{\left[HS_{liq}\right]}{\left[H_2S_{liq}\right]} = pH - pK_{a1}$$
(10)

The pKa $_1$  is ~6.99 at 25 °C [14], and around 6.86 at 31 °C—the operational temperature of the bioreactors [4,13]. Accordingly, the

fraction of non-ionized  ${\rm H_2S_{liq}}$  was estimated based on the total sulfide concentration and corresponding pH. Subsequently, the gas's partial pressure  $(P_{{\rm H_2S_g}})$  was calculated by determining the  ${\rm H_2S}$  concentration in the gas phase. Henry's constant  $(H_{cp})$  at 31 °C was calculated using the Eq. (11).

$$H_{cp} = \frac{\left[ H_2 S_{liq} \right] / M W_{H_2 S}}{P_{H_2 S_a}} \tag{11}$$

where MW $_{\rm H2S}$  represents the molecular weight of H $_2$ S. Correction to 25 °C (298 K) can be done by applying the temperature dependence described by Sander [15], resulting in a 2.28 % increase in the calculated values at 31 °C compared to those at 25 °C.

### 2.7. DNA extraction, sequencing, and taxonomic assignment

Biomass samples for DNA extraction and microbiological analysis were collected from reactor R3 on days #41, #82, and #117, and from R1 on day #105. Briefly, 2 mL of sludge were centrifuged at 7000 g for 5 min, and 250 mg of the resulting pellet was used for total DNA extraction using the DNeasy PowerSoil Pro Kit (Qiagen, Germany), following the manufacturer's instructions. The yield and integrity of all DNA samples were assessed by electrophoresis on 1 % (w/v) agarose gels. 16S rRNA gene PCR amplification and sequencing were conducted by Macrogen (Korea). The V3-V4 region of prokaryotic 16S rRNA gene was amplified primers Bakt 341F (5'-CCTACGGGNGGCWGCAG3') Bakt 805R (5'-GACTACHVGGGTATCTAATCC-3'), and the amplicon library was sequenced on the Illumina MiSeq platform (Illumina, Inc.). Demultiplexed FASTO sequences were pre-processed with cutadapt, trimming reads at both the 5' and 3' ends to ensure a minimum Phred score of Q20. The remaining data were analyzed using the DADA2 plugin within QIIME 2<sup>TM</sup>, which performs paired end read joining, chimera filtering, and clustering into amplicon sequence variants (ASVs). Furthermore, ASVs representing less than 0.001 of the mean sequence count were excluded. Taxonomy was assigned using a classifier trained on the SILVA 16S rRNA database (release 132).

# 2.8. Correlation analysis

Principal component analysis (PCA) and correlation analysis were performed using Python libraries. PCA was carried out with *scikit-learn* library after data standardization with *StandardScaler*. Correlation analysis was visualized as a heatmap using *Seaborn*, with *NumPy*-based triangular masking to highlight key correlations.

# 3. Results and discussion

# 3.1. Biogas production and composition

Fig. 1a and b presents the daily biogas production and composition from the three lab-scale bioreactors, beginning at "day zero". Following a stabilization period, the bioreactors were differentiated according to their feeding compositions (Table 2) and sulfur control strategies. As reported by Weiland [16] and Olivera et al. [13], a noticeable change in the  $CH_4/CO_2$  ratio was observed immediately after the feeding composition was altered (Fig. 1a).

The reactor fed exclusively with BS, represented by R3 until day #43, maintained a  $CH_4/CO_2$  ratio of  $\sim$ 2.8 (composed of approximately 67 %  $CH_4$  and 24 %  $CO_2$ ). In contrast, R2 and R1, which received 50 % and 100 % COD from the SS substrate (see Table 2), exhibited lower ratios of  $\sim$ 2.1 and  $\sim$ 1.6, respectively. On the other hand, biogas production increased from 6.5 L/day in R3 to  $\sim$ 8 L/day in R1 and R2 (Fig. 1b), likely due to higher  $CO_2$  production. After day #43, R3 changed its feed composition to match R1's, resulting in a decline in its  $CH_4/CO_2$  ratio to comparable levels, indicating a similar response to the SS. Meanwhile, R2's operation remained consistent, reaching a steady-state behavior.

# 3.2. Sulfur control strategies and iron dosing. Bioreactors parameters analysis

R1, which received 100 % SS from day zero, showed a marked increase in both liquid and gaseous sulfide concentrations (i.e.,  $\rm H_2S_{liq}/HS_{liq}^-$  and  $\rm H_2S_g)$ . Within the first two weeks, levels reached  $\sim\!500$  mg/L in the liquid phase and  $\sim25,000$  ppm in the gas phase (Fig. 1c and d). A pre-estimated dose of Fe³+ was added then to reduce the sulfide concentration by at least one order of magnitude. One hour later, the liquid sulfide concentration fell to 15 mg/L. Similarly, the  $\rm H_2S_g$  concentration dropped to  $\sim\!5400$  ppm on the next biogas sampling day (i.e., note this value is positively biased, as it included nearly 24 h of sulfide accumulation).

Following the 1st cycle, ending with the iron shock on day #13, sulfide concentrations in R1 gradually increased again as the SLR remained unchanged, reaching peak levels that triggered a 2nd cycle with its own iron shock. In total, five cycles were completed with iron shocks on days #13, #26, #49, #69, and #97. From the 3rd cycle onward, however, the recovery rate of both  ${\rm H}_2{\rm S}_{liq}/{\rm HS}_{liq}^{\rm iq}$  and  ${\rm H}_2{\rm S}_g$  concentrations decreased. Moreover, each iron shock caused a stepwise pH reduction (Fig. 1e), consistent with the high solubility of FeCl<sub>3</sub>, which forms Fe(OH)<sub>3</sub> and releases 3H<sup>+</sup>/mol. After the 5th shock on day #97, the pH dropped below 7, leading to system destabilization and cessation of biogas production.

Conversely,  $SO_4^{2-}$  concentration in R1 remained quite stable throughout the experiment (Fig. 1f, 950  $\pm$  183 mg/L), suggesting that sulfate conversion was unaffected by sulfide precipitation during iron shocks or the associated pH decline. Furthermore, each iron shock caused an immediate increase in biogas volume observed the following day, attributed to the release of additional  $CO_2$  into the biogas. From day zero onward, COD values reflected the transition from BS to SS as feed substrate, stabilizing around 3000 mgCOD/L with a gradual upward trend (Fig. 1g). After the 5th iron shock (day #97), COD increased abruptly, potentially linked to the final pH drop preceding bioreactor collapse (see biogas volume decline in Fig. 1b).

R2 was operated with the same OLR as R1, but received equal contributions from SS and BS, resulting in an SLR of 71.83 mgSO $_q^2$ -/day. L<sub>reactor</sub> —approximately half that of R1 (see Table 2). Initially, both H<sub>2</sub>S<sub>liq</sub>/HS<sub>liq</sub> and H<sub>2</sub>S<sub>g</sub> concentrations increased in proportion to the SLR, showing trends similar to those observed in R1. As reported in [13], the system reached a sulfide steady-state stage between days 15 and 17. Once equilibrium was established, H<sub>2</sub>S<sub>g</sub> and H<sub>2</sub>S<sub>liq</sub>/HS<sub>liq</sub> levels remained relatively constant at 10,497  $\pm$  1467 ppm and 249.5  $\pm$  21.8 mg/L, respectively. No major peaks were observed, suggesting that the SLR was effectively balanced by SRB activity, thus preventing sulfate accumulation during transient stage. This was further reflected in the average SO $_q^2$ - concentrations of 507.9  $\pm$  59.1 mg/L—nearly half that of R1. The pH stabilized at 7.53  $\pm$  0.02, and COD levels remained around 2385  $\pm$  327 mg/L, following an upward trend similar to that observed in R1.

R3 was initially fed with BS until day #43. As shown in Fig. 1c, d, and f, the concentrations of  $\rm H_2S_{liq}/HS_{liq}$ ,  $\rm H_2S_g$  and  $\rm SO_4^{2-}$  remained minimal, reflecting the BS's low sulfur content. This was aligned with favorable biogas parameters (Fig. 1a and b). During this period, pH and COD stayed consistent at ~7.5 and below 2000 mgCOD/mL, respectively (Fig. 1e and g). After switching to 100 % SS on day #43, the concentrations of  $\rm H_2S_{liq}/HS_{liq}$  and  $\rm H_2S_g$  began to mirror R1's. Interestingly, the sulfide accumulation rate in the liquid phase was lower than expected, resembling R1's 4th cycle rather than its 1st (Fig. 1c). Likewise,  $\rm H_2S_g$  in the biogas rose more gradually, surpassing 20,000 ppm at a slower pace (Fig. 1d).

On the other hand,  $SO_4^{2-}$  accumulated in R3 (Fig. 1f), exceeding 3000 mg/L—over three times the equilibrium level in R1. This behavior could be explained by a relatively high Oxidation-Reduction Potential (ORP) in R3, potentially above -150 mV—a level known to inhibit or slow sulfate reduction. Optimal ORP conditions for this process typically range between -200 and -300 mV [6]. By day #83,  $\text{H}_2\text{S}_{liq}/\text{HS}_{liq}^{-}$  and

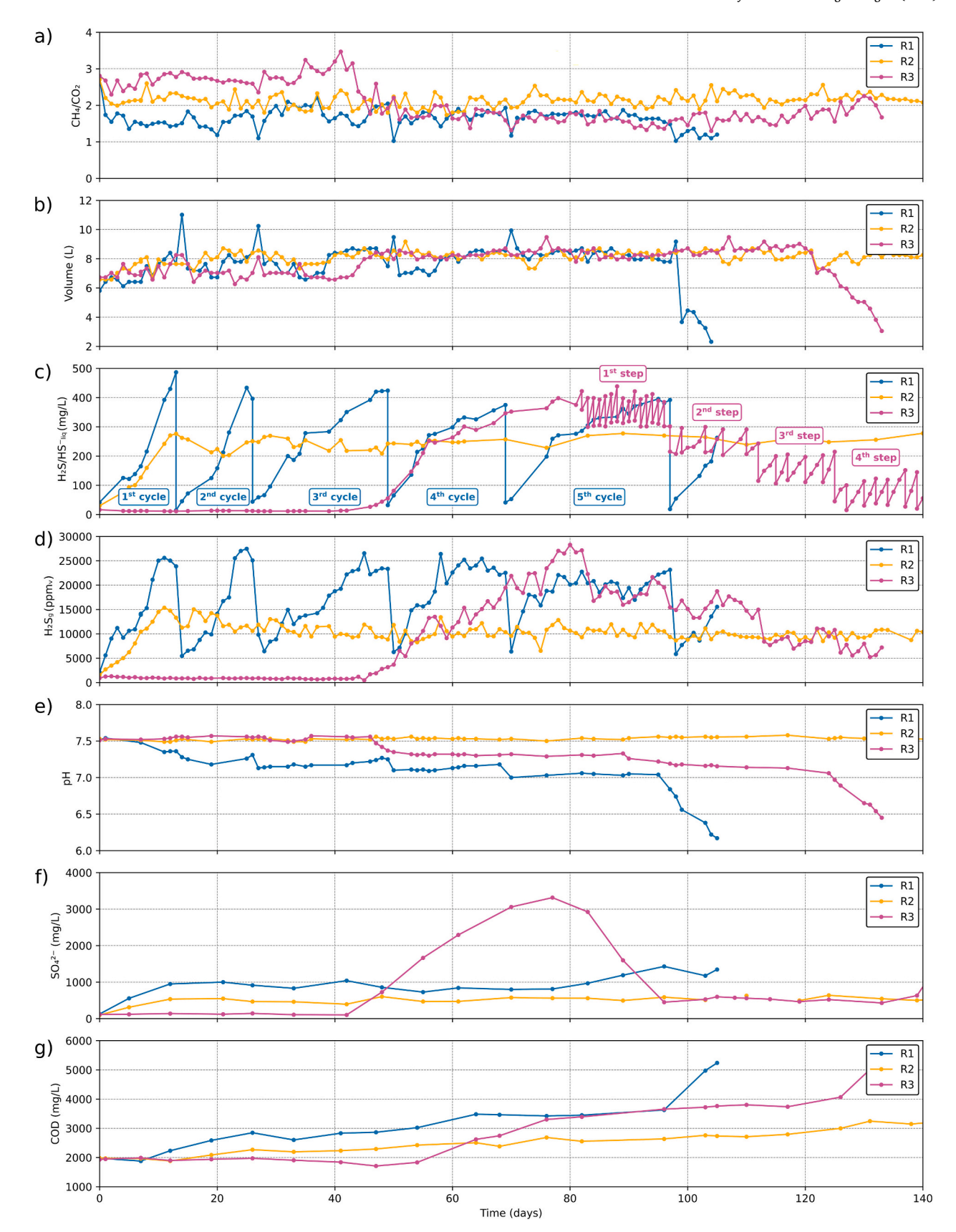


Fig. 1. (a)  $CH_4/CO_2$  ratio and (b) daily biogas production volume. (c) Sulfide concentration in the liquid as  $H_2S_{liq}/HS_{liq}$  (mg/L), (d) hydrogen sulfide in biogas  $H_2S_g$  (ppm<sub>v</sub>) measured after 24 h of accumulation, (e), (f) and (g) pH, sulfate concentration (mg/L) and COD (mg/L) in the liquid, respectively. R1 involved iron shock dosing aimed at complete sulfide precipitation, R2 served as a control without iron addition, and R3 applied a stepwise iron dosing strategy to progressively remove sulfide.

 $\rm H_2S_g$  concentrations achieved 400 mg/L and 25,000 ppm, respectively. At this point, a new iron dosing strategy was implemented in R3. Instead of a single large-dose to precipitate almost all the available sulfide at once, smaller, periodic doses were added to decrease the  $\rm H_2S_{\it liq}/HS_{\it liq}^{\it liq}$  concentration by  $\Delta\approx-100$  mg/L each time, followed by a free recover from  ${\sim}300$  back to  ${\sim}400$  mg/L. This was repeated several times until day #96, marking the 1st step. This approach was performed in a 2nd, 3rd and 4th steps, with sulfide levels varying between  ${\sim}300{-}200$  mg/L (days 97–111),  ${\sim}200{-}100$  mg/L (days 112–124), and  ${\sim}100{-}{<}10$  mg/L (days 125–140), respectively.

During the 1st step, the initial ferric addition likely lowered the ORP, creating favorable conditions for sulfate reduction by SRB. Therefore, the entire sulfate stock in the bioreactor—around 25,500 mg ( $\sim\!3000$  mgSO $^2_4$ /L)—began to be rapidly consumed, along with the daily load (i. e., SLR of 136.1 mgSO $^2_4$ /day.L $_{reactor}$ ). Once the process was unlocked, this great excess of SO $^2_4$  likely exerted pressure on the biological activity of the SRB population, boosting the conversion rate. Consequently, the recovery of those  $\sim\!100$  mg/L of sulfides precipitated by the iron addition was achieved in  $\sim\!24$  h (see Fig. 1c, interval day 83–96). Conversely, once the sulfate stock was depleted and only the SLR remained as input, recovering the same  $\sim\!100$  mg/L took approximately 72 h in the following 2nd, 3rd and 4th steps. As previously discussed, sulfate conversion and its equilibrium concentration appeared to be dependent on the sulfate pressure rather than sulfide levels.

Periodic iron dosing in R3 also caused a gentler drop in pH compared to R1. However, by day #125, the tendency seemed to be broken through pH < 7, resulting in the ceasing of biogas production by day #134. Despite this, both the feeding and the iron dosing were maintained, and  $H_2S_{lig}/HS_{lig}$  measurements continued until day #140.

### 3.3. Sulfur mass balance

Fig. 2 shows the sulfur mass balances for R1, R2, and R3 over different time intervals. The *y*-axis displays total sulfur (S) in mg, averaged daily and normalized per liter of reactor to facilitate comparisons across intervals, reactors, and future studies. The first column indicates the amount of atomic S introduced as  $SO_4^{2-}$  (Eq. (5)). The second and third columns show the S removed from the system (Eq. (6)), either as sulfides ( $H_2S_{liq}/HS_{liq}^{-}$ ) or unchanged sulfates ( $SO_4^{2-}$ ). The fourth column reflects the S released as biogas ( $H_2S_g$ , Eq. (7)). The fifth and sixth columns represent the variation in sulfur content, expressed as mass, due to changes in sulfide and sulfate concentrations within the reactor volume, between a time interval (Eq. (8)). The last column sums all outputs and internal changes (Eq. (9)).

For R1, two-time intervals (i.e., 2nd and 4th cycles) are shown as examples (see Fig. 1c). The percentages in the last column reflect the S mass recovery relative to the input (i.e., the first column). As previously mentioned, iron shocks were applied on the last day of each cycle, allowing mass balance calculations before and after sulfide precipitation in the liquid phase. This effect is illustrated in the last two columns, where downward arrows and dashed areas indicate the substantial impact of these iron shocks on sulfide concentrations within the bioreactor.

Since  $SO_4^{2-}$  levels in the bioreactor remained close to 1000 mg/L during each cycle, over 90 % of the SLR was efficiently converted to sulfides, with about half released as  $H_2S_g$  in the biogas. The shock strategy implemented in R1, successfully reduced the accumulated amount of  $H_2S_{liq}/HS_{liq}$  in the liquid phase. However, it had no impact on the above-mentioned gasified fraction of  $H_2S_g$  already released in the biogas during each prior interval day.

The mass balance for R2 was integrated over the full experiment (up to day #140). As shown in Fig. 2b, about 95 % of the loaded sulfur was

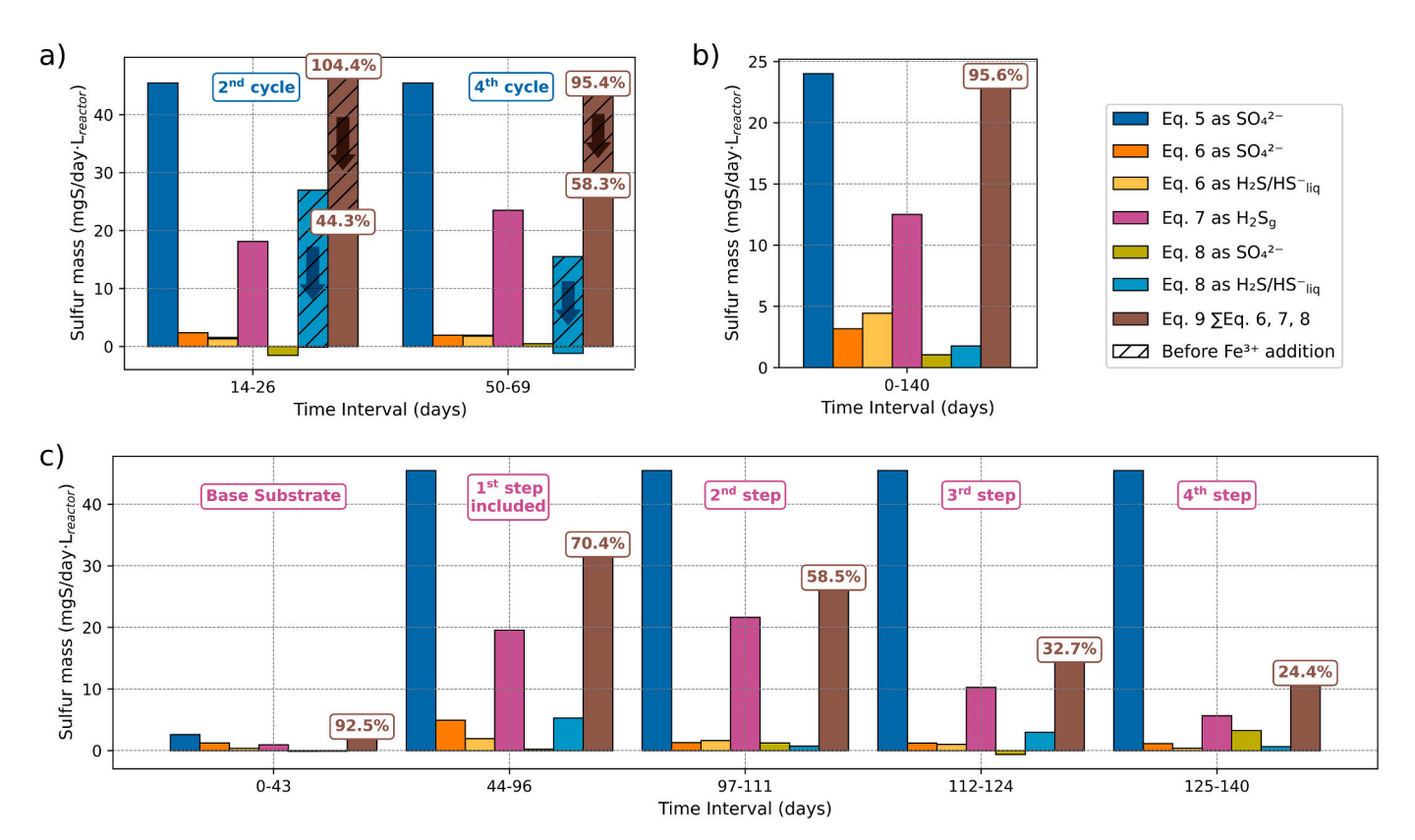


Fig. 2. Elemental S mass balances according to Eq. (9), in terms of its oxidation form (sulfide or sulfate) and Eqs. (5) to (8), at different time intervals. (a) R1: iron added by shocks at the last day of interval. Effects are indicated by arrows. (b) R2: no iron added. (c) R3: iron added stepwise after change in fed at day #43. The percentages indicate S mass recuperation (Eq. (9)/Eq. (5)). Imbalance to 100 % was then related to iron sulfide precipitation (see Fig. 1c).

recovered, confirming the reliability of the analysis. In this steady-state bioreactor,  $\sim$ 78 % of sulfur was converted into sulfides by SRB: 52 % was released as  $\rm H_2S_g$  and 26 % remained in solution as  $\rm H_2S_{\it liq}/\rm HS_{\it liq}^-$  and purged with the digestate.

For R3 (Fig. 2c), the 0–43 day interval (i.e., 100 % BS feed), showed ~90 % sulfur recovery (Eq. (9)). About 49 % of the load was converted into sulfides: 37 % released as  $H_2S_g$  and 12 % remained dissolved ( $H_2S_{liq}/HS_{liq}$ ) and purged with the digestate. From the next interval on, the shift to 100 % SS feed increased the  $SO_4^{2-}$  input, as shown by the height of the first column (Eq. (5)). The 44–96 day interval included  $SO_4^{2-}$  accumulation, consumption, and the initial 1st step of iron dosing (Fig. 1c, d and f). As iron additions continued in each subsequent interval, the sulfur content in the liquid phase ( $H_2S_{liq}/HS_{liq}^{-}$ ), represented by Eqs. (6) and (8), gradually decreased. This decline directly affected the amount of sulfur released as biogas ( $H_2S_g$ , Eq. (7)), following the liquid-gas equilibrium described by Henry's law (Eq. (11)). Finally, the lower recovery percentages observed in the mass balance —except for the first interval with the BS substrate—were linked to the amount of iron added, since the missing sulfur was retained as precipitated sulfide.

### 3.4. Henry's constant analysis

Each bioreactor demonstrated different trends in  $H_{cp}$  values, reflecting the unique physicochemical conditions in each system (Supplementary material Fig. S1). In R2, the  $H_{cp}$  values remained fairly stable at  $1.137 * 10^{-3} \pm 0.207 * 10^{-3}$  mol/m<sup>3</sup> \* Pa, indicating consistent gasliquid equilibrium conditions and showing good agreement with compilated Henry's law constants for hydrogen sulfide [15]. In contrast, R1 exhibited a scattering in  $H_{CD}$  values, mainly a consequence of iron addition. Toward the end of the experiment, as the reactor became acidified, higher  $H_{cp}$  values were obtained —suggesting that lower pH enhances gas release by reducing the solubility of undissociated gas in the liquid phase. Despite the fluctuations from the non-steady sulfide control, the average  $H_{cp}$  in R1 was 1.369 \*  $10^{-3} \pm 0.664 * 10^{-3}$  mol/m<sup>3</sup> \* Pa. In R3,  $H_{cp}$  values were initially low (0.700 \*  $10^{-3} \pm 0.097 * 10^{-3}$ mol/m<sup>3</sup> \* Pa) until day #43, when the feed was switched to 100 % SS. This change resulted in a drop in pH (Fig. 2c), and the  $H_{cp}$  slightly increased (1.324 \*  $10^{-3} \pm 0.263 * 10^{-3} \text{ mol/m}^3 * Pa$ ). Upon the addition of iron on day #82, R3 displayed a related scattering in  $H_{cp}$  values, averaging  $1.492 * 10^{-3} \pm 0.461 * 10^{-3} \text{ mol/m}^3 * Pa$ .

### 3.5. Iron-sulfide relationships

Total sulfide concentrations were measured both before and 1 h after each iron addition: in R1, after the five shock treatments, and in R3, during each gradual dose across the four steps. In R1, linear regression revealed that 1.72 g of iron were required to remove 1 g of sulfide ( $R^2$ 0.99). In contrast, in R3, only 1.14 g of iron were needed to remove 1 g of sulfide ( $R^2 = 0.98$ ) (Fig. 3). When expressed as mole ratios, this corresponds to 0.99 and 0.65 mol of Fe<sup>3+</sup> per mole of sulfide in R1 and R3, respectively, which is remarkably consistent with the stoichiometry formation of FeS and Fe<sub>2</sub>S<sub>3</sub>. However, since Fe<sub>2</sub>S<sub>3</sub> is reported to be unstable [17] and was not directly detected in this study, it can be inferred that when shock dosing is applied, part of the ferric iron ( $\mathrm{Fe}^{3+}$ ) might be consumed in other oxidative processes, leading to the formation of ferrous sulfide (FeS) as the main product (Eq. (2)). When a stepwise dosing of Fe<sup>3+</sup> is applied, Eqs. (3)+(2) or even Eq. (4) seemed to represent the formation of FeS + S<sup>0</sup>, or Fe<sub>2</sub>S<sub>3</sub>, yielding a Fe:S molar ratio of  $\sim 0.66$ .

From both economic and operational perspectives, the R3 gradual dosing method demonstrated improved cost-efficiency by reducing the  ${\rm Fe}^{3+}$  consumption by approximately 580 kg per ton of sulfide removed compared to the R1 strategy. Additionally, R3 simplifies process control by mitigating challenges related to managing hydrogen sulfide concentrations exceeding 20,000 ppm in the biogas, as would occur in the R1 strategy.

# 3.6. Metagenomics analysis

Microbial community shifts in the bioreactors were analyzed by high throughput 16S rRNA sequencing. Samples were taken from R3 on days #41, #82, and #117 (R3–41, R3–82, R3–117) and from R1 on day #105 (R1–105). A total of 398,164 partial sequences were obtained, with an average of  $\sim$ 99,500 reads per sample. Rarefaction curves were generated to evaluate library representativeness, with all samples reaching the plateau before 2000 reads, which indicated adequate sequencing depths. Alpha diversity was highest in R3–41 (BS feed). It dropped in R3–82 with sulfide buildup and declined further in R3–117 and R1–105 as pH fell, reflecting lower richness and evenness (Supplementary Table S1)

The samples revealed a clear shift in microbial composition, marked by bacterial dominance. In R3–41, bacteria accounted for 84 % and

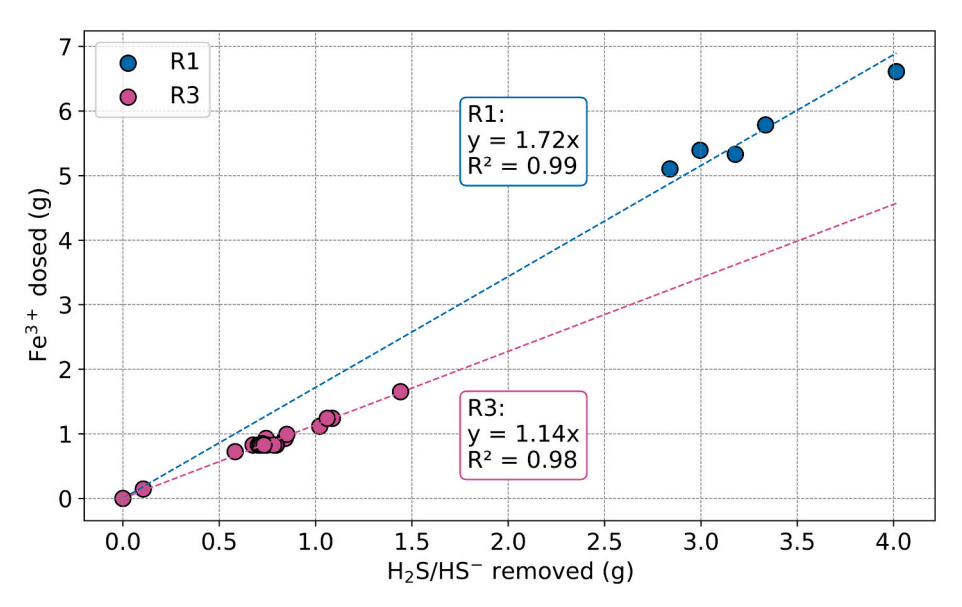


Fig. 3. Relationship between Fe<sup>3+</sup> dosage and sulfur removal as sulfides in bioreactors R1 (with 5 iron shocks achieving almost total sulfide precipitation), and R3 (with iron addition inducing multiple sulfide precipitations of  $\sim$ -100 mg/L, across different step levels). Linear regression analysis yielded Fe<sup>3+</sup>/S ratios of 1.72 gFe<sup>3+</sup>/gS and 1.14 gFe<sup>3+</sup>/gS, respectively.

archaea for 16 %. As conditions changed, bacterial abundance grew to 93 % in R3–82 and R3–117, and further to 97 % in the acidified R1–105, where archaea dropped to 3 %. This trend may result from substrate competition between methanogenic archaea and SRB, along with the greater sensitivity of archaea to sulfide toxicity [18].

All samples presented a similar bacterial community structure, dominated by six main phyla: *Firmicutes* (38.63 % – 53.89 % of the total contigs), *Synergistetes* (4.59 % – 42.69 %), *Bacteroidetes* (5.27 % – 10.29 %), *Spirochaetes* (0.86 % – 7.30 %), *Chloroflexi* (1.18 % – 6.27 %), and *Proteobacteria* (2.47 % – 5.99 %). According to Rivière et al. [19], microorganisms affiliated with *Synergistetes*, *Proteobacteria*, *Bacteroidetes*, and *Chloroflexi* are key members of a core group of phylotypes usually found in most anaerobic digesters. *Synergistetes* tend to thrive under high sulfur loads and low pH, often forming syntrophic relationships with SRB [20]. On the other hand, the Archaea domain, represented by the phylum *Euryarchaeota*, accounted for 2.75–15.18 % of the total contigs.

Taxonomic analysis identified 61 bacterial genera with relative abundances above 1 % in at least one sample (Fig. 4a). Among the most abundant were uncultured members of the *Eubacteriaceae* family (2.33–27.42 % of total bacterial contigs), *Christensenellaceae\_R-7\_group* (0.17–7.72 %), uncultured members of the *Anaerolineaceae* family (0.85–6.23 %), *Syner-01* (2.84–4.73 %), and *Syntrophomonas* (2.08–4.22 %). *Aminobacterium* and *Sporanaerobacter* were only found in R1, representing 29.11 % and 7.44 % of the total bacterial contigs, respectively.

In R3–82 and R3–117, uncultured genera from the *Eubacteriaceae* family showed a marked increase, accounting for nearly 30 % of the bacterial community—considerably higher than in R3–41. This shift likely indicates their involvement in acid fermentation and acetogenesis, potentially driven by the introduction of SS. In contrast, the *Christense-nellaceae\_R-7\_group*, which was dominant in R3–41, declined in R3–82 and R3–117 and was undetectable in R1–105, possibly due to acidic conditions, elevated sulfide concentrations, and competition with SRB and fermentative bacteria such as *Eubacteriaceae*.

Alternatively, R1–105 exhibited a marked increase in the relative abundance of *Aminobacterium* and *Sporanaerobacter*, both known for fermenting amino acids into VFAs. Additionally, *Sporanaerobacter* includes species such as *S. acetigenes*, which are capable of sulfur reduction, suggesting a potential role in extracellular electron transfer [21]. These genera appear to be well-adapted to, or capable of withstanding, the acidified, VFA-rich conditions characteristic of environments like R1–105.

The archaeal community showed considerably lower diversity, with all sequences assigned to just 10 genera (Fig. 4b). Dominant taxa included *Methanobrevibacter* (36.21–56.76 % of total archaea contigs), *Methanospirillum* (4.37–35.80 %), *Candidatus Methanoplasma* (0–27.98 %), and *Methanobacterium* (6.34–26.11 %).

A key difference in the archaeal community was the notable increase in the relative abundance of *Methanobacterium* in R3–82 and R3–117, both exposed to high sulfate loading. These hydrogenotrophic methanogens exhibit enhanced sulfide tolerance and may help maintain community stability under sulfide-induced stress. Similarly, Li et al. [22], reported that *Methanoculleus*, though initially sensitive to sulfide, recovered after prolonged exposure. In this study, its abundance dropped below detection in R3–82 but grew again in R3–117 after 30 days of gradually declining sulfide levels. *Candidatus Methanoplasma*, a methylotrophic archaeon, also increased in R3–82. Although this taxon has been scarcely studied as an essential methanogen in the AD process, it has been linked to lower methane production [23], a phenomenon associated with the SS input in the bioreactors.

In R1–105, *Methanospirillum*, *Candidatus Methanoplasma*, and *Methanobrevibacter* dominated, with the first two showing notable increases in their relative abundances. *Methanospirillum*, in particular, is often found in reactors facing organic overloading and high sulfide concentrations [24].

SRB population dynamics were analyzed given their key role in sulfidogenic anaerobic processes (Fig. 4c). Although overall abundance

remained low (<7 %), a slight increase was detected in R3–82 and R1–105. In R3–82, growth likely responded to high sulfate availability, while in R3–117 it appeared sustained solely by the daily SRL (Fig. 1f).

All identified SRB belonged to the delta-Proteobacteria and Synergistia classes, with most sequences (30.87-50.40 % of total SRB contigs) affiliated with the genus Desulfovibrio. Known for its metabolic versatility, Desulfovibrio can exploit a wide range of electron donors and acceptors, forming syntrophic relationships with methanogenic archaea [25]. Its high affinity for sulfate likely accounts for its dominant presence across nearly all samples analyzed [26]. In R3-41, the SRB community was mainly composed of SEEP-SRB1, a genus known for its role in forming consortia with anaerobic methane-oxidizing archaea, thereby facilitating anaerobic methane oxidation (AOM) [27]. R3-82 showed both higher SRB relative abundance and diversity, with genera like Desulfobulbus and Desulfobotulus becoming detectable, among others. In R3-117, SRB relative abundance declined compared to R3-82, possibly due to reduced sulfide availability caused by iron addition (Fig. 1f). However, Desulfomicrobium slightly increased, probably linked to its syntrophic interaction with Methanolinea, also enriched in this reactor (Fig. 4b) [28]. In the acidified reactor R1–105, the relative abundance of Dethiosulfovibrio increased markedly. This obligately anaerobic, fermentative bacterium thrives in sulfide-rich environments by metabolizing organic compounds under anoxic conditions [29].

### 3.7. Correlation analysis

Operational parameters and analytical measurements were integrated with the metagenomic data through PCA (Fig. 5a). A correlation heatmap was also constructed to illustrate relationships between variables (Fig. 5b).

PCA revealed that the first three components accounted for 50.82%, 29.82%, and 19.36% of the total variance, respectively. The samples were distinctly distributed in the 3D plot, forming a spatial tetrahedron that highlights the compositional differences among R3–41, R3–82, R3–117, and R1–105.

Sample R3-41 was located away from sulfur-related variables and in proximity to methane-related parameters, such as CH4 in biogas and methanogenic archaea (e.g., Methanimicrococcus, Methanobrevibacter), suggesting that the BS feeding condition promoted methane production. This was further supported by the correlation heatmap (Fig. 5b), which showed strong positive correlations between CH<sub>4</sub> and Methanimicrococcus (r = 0.95) as well as Methanobrevibacter (r = 0.99). As expected, both methanogens were negatively correlated with sulfur species, including  $H_2S_{liq}/HS_{liq}^-$  concentration (r = -0.74 and -0.70),  $H_2S_g$  concentration (r = -0.75 and -0.68), and S input (r = -1.00 and -0.92). R3–41 also showed a strong association with SEEP-SRB1, which exhibited significant positive correlations with Methanobrevibacter (r =0.98) and *Methanimicrococcus* (r = 0.94), suggesting potential syntrophic interactions, like those described for SEEP-SRB1a and ANME-2 archaea [30]. Additionally, sample R3-41 was associated to Christensenellaceae R-7 group, whose abundance declined with decreasing pH (r =0.73) and was undetectable in R1-105.

The sample R3–82 was located at the upper-corner of the tetrahedral figure in the PCA plot, highly related to  $SO_4^{2-}$  concentrations, reflecting its accumulation in the system (Fig. 1f). It was also situated close to  $H_2S_{liq}/HS_{liq}$  and  $H_2S_g$  vectors. As expected, R3–82 showed strong associations with SRB such as *Desulfobotulus*, *Desulfobulbus* and *Desulfocurvus*, whose relative abundances notably increased in this sample (Fig. 4c).

R3–117, in the lower-corner of the PCA plot, was linked to *Methanoculleus* and, to a lesser extent, *Methanobacterium*. The addition of Fe<sup>3+</sup> helped mitigate sulfide toxicity, leading to an increase in the relative abundance of *Methanoculleus* (Fig. 4b). This trend was supported by its negative correlation with  ${\rm H}_2{\rm S}_{liq}/{\rm HS}_{liq}^-$  (r=-0.84) and  ${\rm H}_2{\rm S}_g$  (r=-0.83) concentrations. *Desulfomicrobium* was also present and associated with R3–117. The strong positive correlation observed between

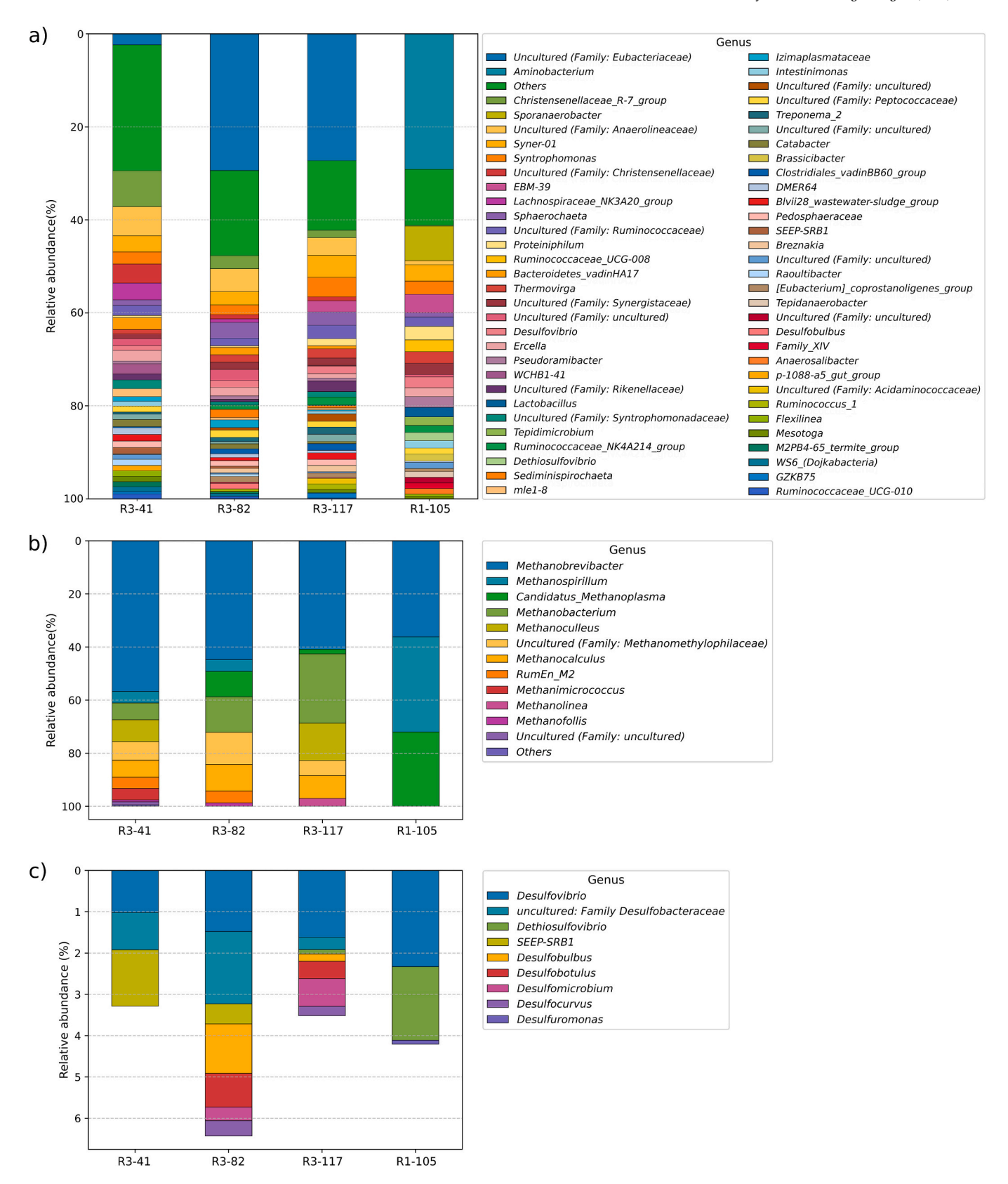


Fig. 4. Taxonomic classification at genus level for bacteria (a), archaea (b), and SRB (c) in bioreactor R3 (R3–41, R3–82 and R3–117), as well as in R1 (R1–105). For (a) and (b), sequences representing less than 1 % of the population were grouped under the category "Others."

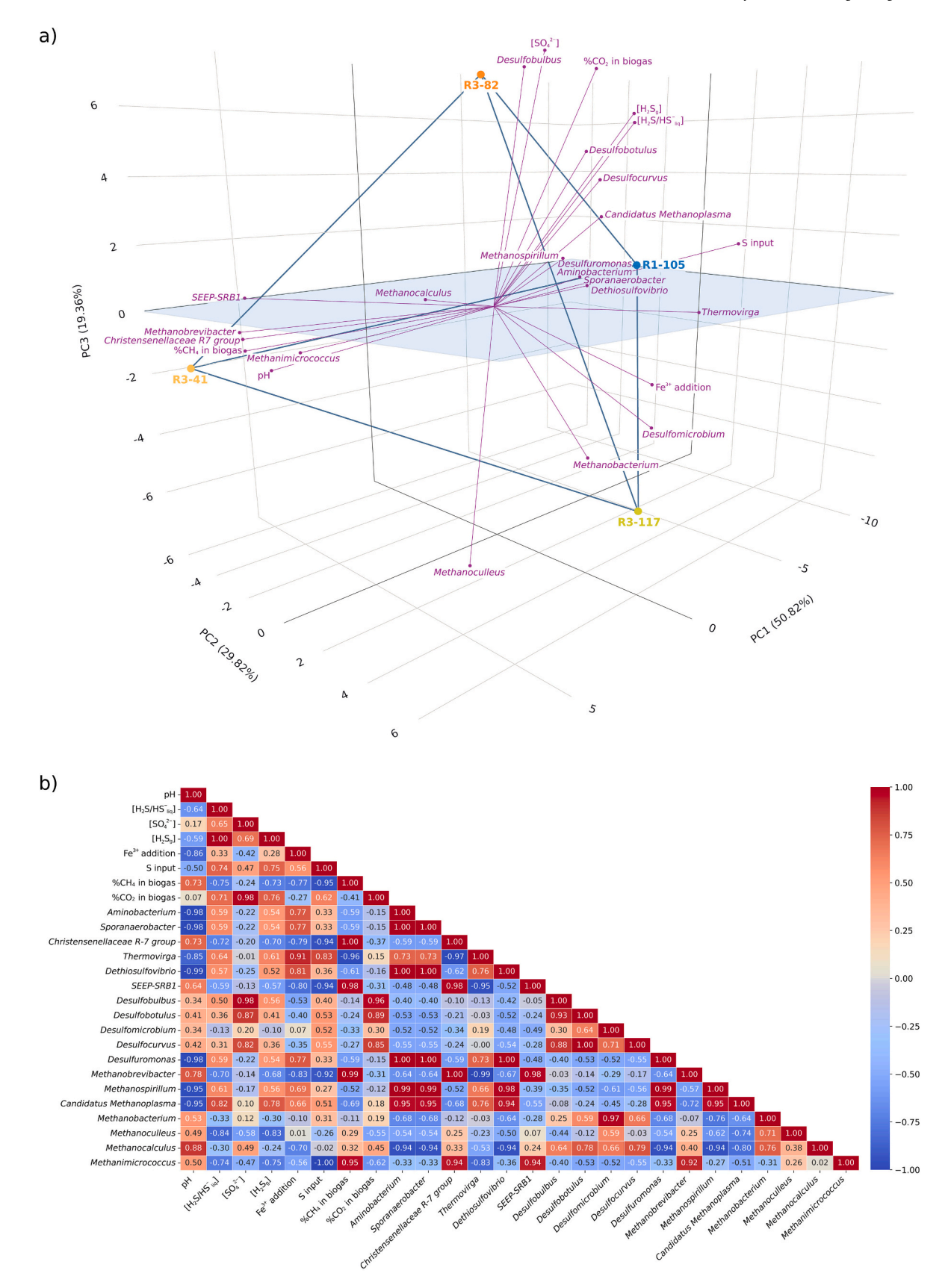


Fig. 5. (a) PCA plot and (b) correlation map illustrating relationships between parameter pairs. The interactive PCA plot is available online at https://pca2public.stre amlit.app.

Methanobacterium and Desulfomicrobium (r = 0.97) suggests a potential syntrophic relationship between these hydrogenotrophic methanogens and SRB.

Finally, R1-105 in the remaining corner of the PCA plot, was aligned with H<sub>2</sub>S<sub>lig</sub>/HS<sub>lig</sub> and H<sub>2</sub>S<sub>g</sub> concentrations, underscoring—as previously discussed—the strong influence of sulfide-related variables at this stage. R1-105 exhibited a notable association with Aminobacterium, Sporanaerobacter, and Dethiosulfovibrio. Its placement opposite the pH vector highlights the acidic conditions that characterized this sample. This was further supported by the heatmap, which revealed negative correlations between these genera and pH (r = -0.98, -0.98, and -0.99, respectively). The proximity of Methanospirillum and Candidatus Methanoplasma to R1-105 suggests that hydrogenotrophic methanogenesis played a prominent role under these conditions, likely as an adaptation to the acidic and sulfide-rich environment. Both methanogens exhibited strong negative correlations with pH (r = -0.95 each), and positive correlations with *Dethiosulfovibrio* (r = 0.98 and 0.94, respectively) and Desulfuromonas (r = 0.99 and 0.95, respectively), also closely related to R1–105. However, Methanospirillum and Candidatus Methanoplasma showed moderate negative correlations with  $CH_4$  production (r = -0.52and - 0.69, respectively), suggesting that although they thrive under acidic conditions, their abundance may be inversely related to methane yield. Moreover, R1-105 was closely associated with Thermovirga, a genus capable of utilizing elemental sulfur-generated during sulfide oxidation mediated by Fe<sup>3+</sup> —as an electron acceptor [31]. Notably, *Thermovirga* exhibited a strong positive correlation with  $Fe^{3+}$  addition (r= 0.91) and S input (r = 0.83), reinforcing its reliance on these substrates for growth. Conversely, it was negatively correlated with pH (r =-0.85) and CH<sub>4</sub> in biogas (r = -0.96), reflecting both its adaptation to acidic conditions and its prevalence in environments with diminished methane production.

Both R1–105 and R3–117 were related to the Fe<sup>3+</sup> addition vector, which itself displayed a negative correlation with pH (r=-0.86), further highlighting the acidifying effect of iron treatment on reactor conditions.

# 4. Conclusions

This study evaluated the performance of two ferric dosing strategies for sulfide control in anaerobic bioreactors subjected to high sulfate loads. The stepwise-dosing approach required a lower Fe<sup>3+</sup>/S<sup>2-</sup> molar ratio (0.65) compared to shock-dosing (0.99), suggesting the formation of insoluble FeS + S<sup>0</sup> and/or Fe<sub>2</sub>S<sub>3</sub> instead of only FeS. While iron addition effectively mitigated sulfide accumulation, it also induced acidification, which ultimately inhibited methanogenesis and biogas production. The sulfur mass balance highlighted that sulfate pressure accelerated the SRB activity. At a low SLR of 7.58 mgSO $_4^{2-}$ /day.L<sub>reactor</sub>, only 49 % of sulfate was converted into sulfides, whereas higher SLRs of 71.83 and 136.1 mgSO $_4^{2-}$ /day.L<sub>reactor</sub> led to conversions of 78 % and 90 %, respectively. Acidification also resulted in a slight increase in Henry's constants. High-throughput sequencing analysis revealed a decline in alpha diversity, especially in environments characterized by increased acidity and elevated sulfide levels. SRB communities thrived under sulfate-rich conditions, while methanogenic archaea were progressively inhibited under the acidic environment induced by ferric iron dosing.

### CRediT authorship contribution statement

Valentina Girardi: Writing – review & editing, Writing – original draft, Visualization, Software, Methodology, Investigation, Formal analysis, Data curation, Conceptualization. María Laura Tondo: Writing – review & editing, Writing – original draft, Visualization, Validation, Supervision, Methodology, Investigation, Funding acquisition, Formal analysis, Data curation. Cecilia Lucía Balaban: Writing – review & editing, Visualization, Validation, Supervision, Software, Methodology, Investigation, Data curation. María Sol Herrero: Writing

original draft, Validation, Supervision, Methodology, Investigation, Funding acquisition, Data curation, Conceptualization. Camila Olivera:
 Software, Methodology, Investigation, Formal analysis, Data curation.
 Lucas Matías Salvatierra: Writing – review & editing, Writing – original draft, Visualization, Validation, Supervision, Resources, Project administration, Methodology, Investigation, Funding acquisition, Formal analysis, Data curation, Conceptualization.

### **Funding**

This work was supported by grants ANPCyT PICT-335-2021 and PICyT 017-A-2021 UCA.

### **Declaration of competing interest**

The authors declare that they have no known competing financial interests or personal relationships that could have appeared to influence the work reported in this paper.

### Acknowledgements

The authors extend their gratitude to the National Research Council of Argentina (CONICET) for providing scientific fellowships to V.G. and C.O., as well as research positions to M.L.T., C.L.B., and L.M.S. Additionally, they acknowledge the Pontifical Catholic University of Argentina for supporting research positions (M.S.H.) and for hosting laboratories and facilities at the INGEBIO Institute. Finally, the authors express their appreciation to SOLAMB SRL for supplying the samples.

## Appendix A. Supplementary data

Supplementary data to this article can be found online at https://doi. org/10.1016/j.jwpe.2025.108405.

## Data availability

Data will be made available on request.

### References

- [1] J. Wu, Q. Niu, L. Li, Y. Hu, C. Mribet, T. Hojo, Y.Y. Li, A gradual change between methanogenesis and sulfidogenesis during a long-term UASB treatment of sulfaterich chemical wastewater, Sci. Total Environ. 636 (2018) 168–176, https://doi. org/10.1016/j.scitotenv.2018.04.172.
- [2] C. Yongsiri, S.M. Asce, J. Vollertsen, T. Hvitved-Jacobsen, Influence of wastewater constituents on hydrogen sulfide emission in sewer networks, J. Environ. Eng. 131 (2004) 1676–1683, https://doi.org/10.1061/ASCE0733-93722005131:121676.
- [3] Y. Chen, J.J. Cheng, K.S. Creamer, Inhibition of anaerobic digestion process: a review, Bioresour. Technol. 99 (10) (2008) 4044–4064, https://doi.org/10.1016/j. biortech.2007.01.057.
- [4] F.J. Millero, The thermodynamics and kinetics of the hydrogen sulfide system in natural waters, Mar. Chem. 18 (2–4) (1986) 121–147, https://doi.org/10.1016/ 0304-4203(86)90003-4.
- [5] I. Díaz, A.C. Lopes, S.I. Pérez, F. Fdz-Polanco, Performance evaluation of oxygen, air and nitrate for the microaerobic removal of hydrogen sulphide in biogas from sludge digestion, Bioresour. Technol. 101 (2010) 7724–7730, https://doi.org/ 10.1016/j.biortech.2010.04.062.
- [6] A.H. Nielsen, P. Lens, J. Vollertsen, T. Hvitved-Jacobsen, Sulfide-iron interactions in domestic wastewater from a gravity sewer, Water Res. 39 (2005) 2747–2755, https://doi.org/10.1016/j.watres.2005.04.048.
- [7] B. Kiilerich, A.H. Nielsen, J. Vollertsen, Kinetics of sulfide precipitation with ferrous and ferric iron in wastewater, Water Science & Technol. 78 (5–6) (2018) 1071–1081. https://doi.org/10.2166/wst.2018.382.
- [8] B. Yu, D. Zhang, A. Shan, Z. Lou, H. Yuan, X. Huang, W. Yuan, X. Dai, N. Zhu, Methane-rich biogas production from waste activated sludge with the addition of ferric chloride under a thermophilic anaerobic digestion system, RSC Adv. 5 (2015) 38538–38546, https://doi.org/10.1039/C5RA02362A.
- [9] ASCE, Sulfide in wastewater collection and treatment systems, in: Manuals and Reports on Engineering Practice N.69, American Society of Civil Engineers, New York, USA, 1989.
- [10] A.H. Nielsen, T. Hvitved-Jacobsen, J. Vollertsen, Effects of pH and iron concentrations on sulfide precipitation in wastewater collection systems, Water Environ. Res. 80 (2008) 380–384, https://doi.org/10.2175/106143007X221328.

- [11] J.S. Lar, X. Li, Removal of H<sub>2</sub>S during anaerobic bioconversion of dairy manure, Chin. J. Chem. Eng. 17 (2) (2009) 273–277, https://doi.org/10.1016/S1004-9541 (20)2025 0
- [12] D. Erdirencelebi, M. Kucukhemek, Control of hydrogen sulphide in full-scale anaerobic digesters using iron (III) chloride: performance, origin and effects, Water SA 44 (2) (2018), https://doi.org/10.4314/wsa.v44i2.04.
- [13] C. Olivera, M.L. Tondo, V. Girardi, L. Fattobene, M.S. Herrero, L.M. Pérez, L. M. Salvatierra, Early-stage response in anaerobic bioreactors due to high sulfate loads: hydrogen sulfide yield and other organic volatile sulfur compounds as a sign of microbial community modifications, Bioresour. Technol. (2022) 126947, https://doi.org/10.1016/j.biortech.2022.126947.
- [14] APHA, Standard Methods for the Examination of Water and Wastewater, 23rd ed., American Public Health Association, Washington, DC, USA, 2017.
- [15] R. Sander, Compilation of Henry's law constants (v5.0.0) for water as solvent, Atmos. Chem. Phys. 23 (2023) 10901–12440, https://doi.org/10.5194/acp-23-10901-2023
- [16] P. Weiland, Biogas production: current state and perspectives, Appl. Microbiol. Biotechnol. 85 (4) (2010) 849–860, https://doi.org/10.1007/s00253-009-2246-7.
- [17] V.V. Onufrienok, Metastable iron sulfides, Inorg. Mater. 41 (6) (2005) 650–653, https://doi.org/10.1007/s10789-005-0184-z.
- [18] Y. Cai, Z. Zheng, X. Wang, Obstacles faced by methanogenic archaea originating from substrate-driven toxicants in anaerobic digestion, J. Hazard. Mater. 403 (2021) 123938, https://doi.org/10.1016/j.jhazmat.2020.123938.
- [19] D. Rivière, V. Desvignes, E. Pelletier, S. Chaussonnerie, S. Guermazi, J. Weissenbach, T. Li, P. Camacho, A. Sghir, Towards the definition of a core of microorganisms involved in anaerobic digestion of sludge, ISME J. 3 (6) (2009) 700–714, https://doi.org/10.1038/ismej.2009.2.
- [20] A. El Houari, M. Ranchou-Peyruse, A. Ranchou-Peyruse, R. Bennisse, R. Bouterfas, M.S. Goni Urriza, A.-I. Qatibi, R. Guyoneaud, Microbial communities and sulfate-reducing microorganisms abundance and diversity in municipal anaerobic sewage sludge digesters from a wastewater treatment plant (Marrakech, Morocco), Processes 8 (2020) 1284, https://doi.org/10.3390/pr8101284.
- [21] G. Hernandez-Eugenio, M.-L. Fardeau, J.-L. Cayol, B.K. Patel, P. Thomas, H. Macarie, J.-L. Garcia, B. Ollivier, Sporanaerobacter acetigenes gen. nov., sp. nov., a novel acetogenic, facultatively sulfur- reducing bacterium, Int. J. Syst. Evol. Microbiol. 52 (4) (2002) 1217–1223. https://pubmed.ncbi.nlm.nih.gov/ 12148631/
- [22] J. Li, H.Z. Wang, Y. Yi, Z.Y. Zhao, X.H. Liu, J. Xu, X.W. Peng, Response of isovalerate-degrading methanogenic microbial community to inhibitors, Appl.

- Biochem. Biotechnol. 191 (3) (2020) 1010–1026, https://doi.org/10.1007/s12010-020-03234-9
- [23] E.C.G. Vendruscolo, D. Mesa, D. Vasconcelos Rissi, B.H. Meyer, F. de O. Pedrosa, E. Maltempi de Souza, L. Magalhães Cruz, Microbial communities network analysis of anaerobic reactors fed with bovine and swine slurry, Sci. Total Environ. 742 (2020) 140314, https://doi.org/10.1016/j.scitotenv.2020.140314.
- [24] V.K. Tyagi, A. Bhatia, K. Kubota, A. Rajpal, B. Ahmed, A.A. Khan, A.A. Kazmi, M. Kumar, Microbial community dynamics in anaerobic digesters treating organic fraction of municipal solid waste, Environ. Technol. Innov. 21 (2021) 101303 (10.1016/j.eti.2020).
- [25] I.P. Pankhania, Hydrogen metabolism in sulphate-reducing bacteria and its role in anaerobic corrosion, Biofouling 1 (1) (1988) 27–47, https://doi.org/10.1080/ 08027018809378004
- [26] G. Muyzer, A.J.M. Stams, The ecology and biotechnology of sulphate-reducing bacteria, Nat. Rev. Microbiol. 6 (6) (2008) 441–454, https://doi.org/10.1038/ prmicro1802
- [27] T. Watanabe, K. Kubo, Y. Kamei, H. Kojima, M. Fukui, Dissimilatory microbial sulfur and methane metabolism in the water column of a shallow meromictic lake, Syst. Appl. Microbiol. 45 (3) (2022) 126320, https://doi.org/10.1016/j. systp. 2023 126320.
- [28] J. Kim, H. Jung, C. Lee, Shifts in bacterial and archaeal community structures during the batch biomethanation of *Ulva* biomass under mesophilic conditions, Bioresour. Technol. 169 (2014) 502–509, https://doi.org/10.1016/j. biortech 2014 07 041
- [29] E. Cytryn, I. Gelfand, Y. Barak, J. van Rijn, D. Minz, Diversity of microbial communities correlated to physiochemical parameters in a digestion basin of a zero-discharge mariculture system, Environ. Microbiol. 5 (2003) 55–63, https://doi.org/10.1046/i.1462-2920.2003.00392.
- [30] L. Schreiber, T. Holler, K. Knittel, A. Meyerdierks, R. Amann, Identification of the dominant sulfate-reducing bacterial partner of anaerobic methanotrophs of the ANME-2 clade, Environ. Microbiol. 12 (8) (2010) 2327–2340, https://doi.org/ 10.1111/j.1462-2920.2010.02275.x.
- [31] S. Shakeri Yekta, R.M. Ziels, A. Björn, U. Skyllberg, J. Ejlertsson, A. Karlsson, M. Svedlund, M. Willen, B.H. Svensson, Importance of sulfide interaction with iron as a regulator of the microbial community in biogas reactors and its effect on methanogenesis, volatile fatty acids turnover, and syntrophic long-chain fatty acids degradation, JBB 123 (5) (2017) 597–605, https://doi.org/10.1016/j. ibiosc.2016.12.003.